

Nonequilibrium molecular dynamics simulation of the in-plane thermal conductivity of superlattices with rough interfaces

Konstantinos Termentzidis* and Patrice Chantrenne

Centre de Thermique de Lyon CETHIL UMR5008, Université de Lyon, INSA de Lyon, CNRS, Université Lyon 1, Lyon F-69621, France

Pawel Koblinski

Department of Materials Science and Engineering, Rensselaer Polytechnic Institute (RPI), Troy, New York 12180, USA

(Received 18 March 2009; revised manuscript received 28 May 2009; published 30 June 2009)

We report nonequilibrium molecular dynamics study of heat transfer in binary Lennard-Jones superlattices. The influence of the characteristic height of the interface roughness and the superlattice period on the in-plane thermal conductivity is reported. We observe that in-plane thermal conductivity first decreases with an increase in the characteristic height of the roughness. For perfectly periodic roughness, it seems that the thermal conductivity exhibit a minimum value when the characteristic height of the roughness becomes comparable with the superlattice period.

DOI: [10.1103/PhysRevB.79.214307](https://doi.org/10.1103/PhysRevB.79.214307)

PACS number(s): 47.11.Mn, 74.25.Fy, 74.78.Fk

I. INTRODUCTION

Superlattices are structures composed of alternating layers of two or more different materials arranged either randomly or periodically.¹ The most studied superlattices are those composed of two materials with a certain degree of periodicity. The interest in superlattices arises because they exhibit new combinations of material properties as, for example, their low thermal conductivity, λ (Ref. 2). This makes superlattices promising materials for applications in devices such as semiconductor lasers,³ optical data-storage media,⁴ thermoelectric,^{5,6} and thermomechanic devices,⁷ where the thermal-conductivity characteristics is important for the device operation.⁸

Thermal conductivity of the superlattice depends on many factors. In bulk materials, the temperature affects thermal conductivity mainly by controlling the intrinsic phonon mean-free path. The periodicity of the superlattice modifies the phonon-dispersion relation and more specifically the group velocity of phonons due to zone folding.^{9,10} Furthermore, interfacial roughness plays an important role.¹¹ All these factors typically lead to the cross-plane thermal conductivity of superlattices being at least 1 order-of-magnitude smaller than the thermal conductivity of the bulk materials that form the superlattice.¹² This reduction has been explained by zone folding or more specifically the formation of the mini-Brillouin zone—the so-called mini-umklapp three-phonon-scattering process¹³—that causes a reduction in the group velocity of phonons.¹¹ Alternative to zone-folding picture is one based on phonon scattering at interfaces. In this case some authors claim that this reduction is caused by a complete diffusive phonon scattering,^{14,15} while others cite the acoustic mismatch difference and phonon filtering.¹⁶ Phonon filtering occurs when phonons of wavelength λ_0 satisfy the Bragg condition $\lambda_0 = 2d_0$ (where d_0 is the superlattice period).^{17,18} Li *et al.*¹⁹ performed a systematic study on $\text{Si}_x\text{Ge}_{1-x}/\text{Si}_y\text{Ge}_{1-y}$, and showed that the influence of the x/y ratio on the phenomena is related to the behavior of phonons at the surfaces. Simkin and Mahan²⁰ distinguished two regions where the phonons should be treated as waves or par-

ticles, depending on whether the layers are thinner than the phonon mean-free path or not. Thermal conductivity is also affected by the level of doping of the superlattices.^{21,22}

An intriguing effect in the simulated cross-plane thermal conductivity of superlattices is the appearance of a minimum for superlattice periods of 8 to 10 monolayers, in contrast to experimental results.^{8,23–28} The reason for the discrepancy between experiment and theory is claimed to be due to the quality of the interfaces.¹² Volz *et al.*²⁹ also mentioned the problem of the unpredictable behavior of heat carriers at the rough interfaces because of the complexity of the phonons reflection mechanism (mode conversion, inelastic scattering, angular, and wavelength dependency). In support of this argument simulations of smooth interface superlattice showed the appearance of a minimum in the thermal conductivity due to miniband formation²⁶ while this trend disappears for rough interfaces. This can explain the absence of a minimum in the experiments. This minimum occurs when the phonon mean-free path is of the same order as the superlattice period length and the lattice constants of the two materials that form the superlattices are very close to each other. Simulations also demonstrated that surface stress due to lattice mismatch greater than 4% leads to the disappearance of a minimum in the thermal conductivity. In a recent study, Donadio and Galli found that nanowire's thermal conductivity strongly depends on the nature of the surface structure (more or less amorphous).³⁰

Marty *et al.*^{31,32} developed a new method to manufacture deep silicon trenches with submicron feature sizes (Fig. 1). The height and periodicity of the wavelike shape of the surfaces can be monitored. When the trenches are filled in with another material, they give rise to superlattices with interfaces whose roughness can be modeled with periodic geometry. These new nanostructured materials are good candidates for nanophotonic and thermoelectric applications. For the latest, it is then important to optimise the roughness characteristic sizes to get the lowest thermal conductivity. In our investigation we will focus on systematic exploration of the role of the interfacial roughness on in-plane thermal conductivity. While prior simulation studies show thermal-

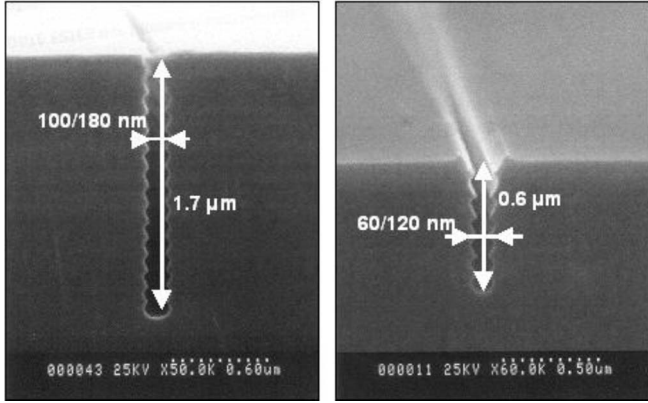


FIG. 1. SEM pictures obtained by the group ESYCOM and ESIEE at Marne-la-Vallée, France, showing two submicron tranches in a silicon wafer.

conductivity reduction due to roughness,^{14,33,34} the roughness studied was limited to a couple of atomic layers. In the current study we vary the interfaces roughness from a single atomic layer to values even greater than the half of superlattice period. Perfectly periodic geometries and randomlike geometries of interface's roughness will be considered.

The main aim of our current work is to elucidate the interplay between various lengths involved in the thermal transport including (i) the characteristic height of the roughness of the superlattice interfaces, (ii) the superlattice period, and (iii) intrinsic phonon mean-free path of bulks materials forming the interface. Motivated by the experiment^{31,32} as shown in Fig. 1 we will focus on the periodic-roughness structures. However, for comparison we will consider similar structures but with random roughness.

This paper is organized as follows: in Sec. II, model systems, nonequilibrium molecular dynamics (NEMD) method, and the methodology to determine the thermal conductivity of the superlattices is described. In Sec. III the results on in-plane thermal conductivity of superlattices and associated thin films are presented and compared against prediction of a continuous analysis. The last section contains the conclusions and a discussion of the future research.

II. MOLECULAR DYNAMICS SIMULATION

A. Nonequilibrium molecular dynamics method

There are three principal techniques used to evaluate the thermal conductivity via molecular dynamic simulations;³⁵ (i) the equilibrium approach based on the Green-Kubo method,³⁶ (ii) heat source and sink, also called direct method, NEMD based on the creation of temperature gradient, (iii) and the homogeneous NEMD, where a heat flux is induced, however, without a temperature gradient thus allowing to use periodic boundary conditions in a similar manner as in the equilibrium approach.^{37,38}

The direct method, proposed by Kotake and Wakuri,³⁹ is similar to the hot-plate experiment setup. A temperature gradient is imposed across the structure under study by imposing thermal power exchange between heat source and sink

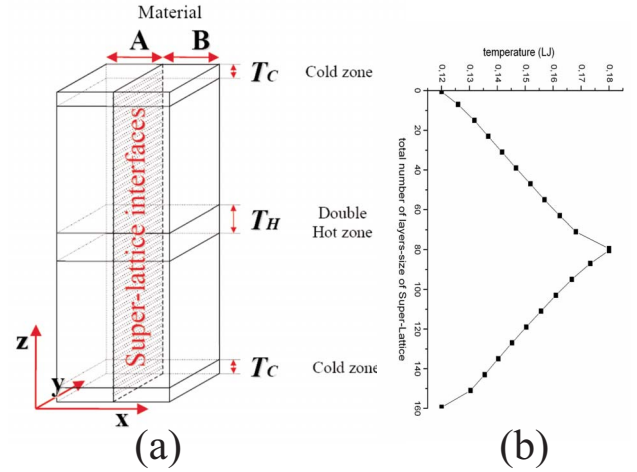


FIG. 2. (Color online) (a) Geometric configuration to simulate heat transfer with periodic boundary conditions. (b) Example of a temperature profile of the system in the z direction with cold source at $T_C=0.12$ (LJ) and hot at $T_H=0.18$ (LJ).

and measure the resulting heat flux.^{40,41} An alternative, but equivalent way is to induce a heat flux and to measure the resulting temperature gradient.⁴² In both cases the system is first allowed to reach a steady state, after which a prolong simulations are conducted allowing to obtain correct statistical measurements.⁴³ The NEMD method is often the method of choice for studies of nanomaterials⁴¹ while for bulk thermal conductivity, particularly of high-conductivity materials, equilibrium method is typically preferred due to less severe size effects. The comparison between the two methods were undertaken by many researchers, with a main conclusion that the two methods give consistent with each other results.^{41,44–47}

B. Simulation setup

The basic geometry for in-plane conductivity simulations is presented in Fig. 2. The heat flux is imposed along the z direction. Periodic boundary conditions are used in all directions. The planar-slab heat source is located at the center of the simulation cell, while heat sink is located at the edges. With periodic boundary conditions employed, the resulting steady-state temperature profile is symmetric about the center normal to z plane. To study the in-plane thermal conductivity, half of the simulation cell is made of material A and the other half by the material B with the interfaces normal to x direction. Figure 2(b) shows the typical temperature gradient across the structure.

The molecular dynamics code LAMMPS (Refs. 48–50) is used in all NEMD simulation. For the description of interatomic interactions, Lennard-Jones (LJ) potential is used. The later is justified by our interest in the main phenomena introduced to the thermal conductivity by the interfaces. More realistic potentials are planned to be used in the future. All calculations have been performed with structures first equilibrated at a temperature of 0.15 (in reduced LJ units). For all calculations the LJ energy unit $\epsilon_{ij}=1.0$ and length unit $\sigma_{ij}=1.0$ are used. In consequence the two materials, which

form the superlattice have the same lattice constants and effective elastic constants. They only differ by the mass of the atoms with mass ratio equal to 2.0. This ratio lead to the acoustic impedance ($Z=\rho_0c$, where ρ_0 is density and c is the speed of sound⁵¹) ratio of $\sqrt{m_2/m_1}$ which is similar the impedance ratio as that of silicon and germanium ($\frac{Z_{Si}}{Z_{Ge}} \sim 1.78$).

The ratio of the acoustic impedance of the two media determines reflection and transmission coefficient of acoustic phonons across the interface and thus greatly impact the efficiency of the energy transfer and superlattice conductivity. A similar simulations setup with a mass ratio of 1:4 and the same LJ parameters was used by Stevens *et al.*³⁴ to perform molecular dynamic simulations of the energy transfer across an interface.

In all simulation we use the molecular dynamics time step of 0.001 (LJ time units). The calculated temperatures and energy flux are averaged over a large number of time steps (1–20 million steps), after the steady state is established. The steady state is attained after about 100.000 time steps for the small systems, while for the largest ones 0.5–1 million time steps are required. After reaching this state we collect the temperature profiles and monitor the heat power of the source and sink over several millions time steps, in order to achieve a good statistical accuracy. The knowledge of the heat flux and the temperature profile allows one to determine the thermal conductivity using the Fourier's law,

$$j = -\lambda \frac{dT}{dx}, \quad (1)$$

where λ is the thermal conductivity and dT/dx is the gradient of the temperature.

In all simulations the average temperature of the system is kept constant at 0.15 (LJ) while it is achieved by maintaining the heat sink at 0.12 (LJ) and the source at 0.18 (LJ). These temperatures are well below the triple point and thus represent a typical inorganic solid and ambient. Furthermore, at $T=0.15$ (LJ) a phonon mean-free path of the bulk material is comparable to the superlattice periods used in our simulations. The influence of the size of the hot and cold baths [Fig. 2(a) areas T_C , T_H] is negligible as only minor quantitative changes occur in thermal conductivity. After the above verification, all the calculations have been done using a thermostat size of four monolayers.

Figure 3 illustrates the method used to determine the thermal conductivity of a system with a specific roughness. The system size is given by $n_x \times n_y \times n_z$, where n_x , n_y , or n_z are the number of lattice parameter in the x , y , or z direction. For each specific roughness, simulations were performed for at least four structures with different sizes in the z direction. In the example of Fig. 3, z dimension of the structures that have been studied are 20, 40, 80, and 160. For each size, the steady-state heat-transfer rate and temperature gradient is determined from which the thermal conductivity have been calculated. The method proposed in Refs. 41 and 52 was used to calculate the uncertainties in temperature and heat flux. Then, as suggested by Schelling *et al.*,⁴⁵ by plotting the inverse of the thermal conductivity as a function of the inverse of the system size in the z direction, the thermal conductivity

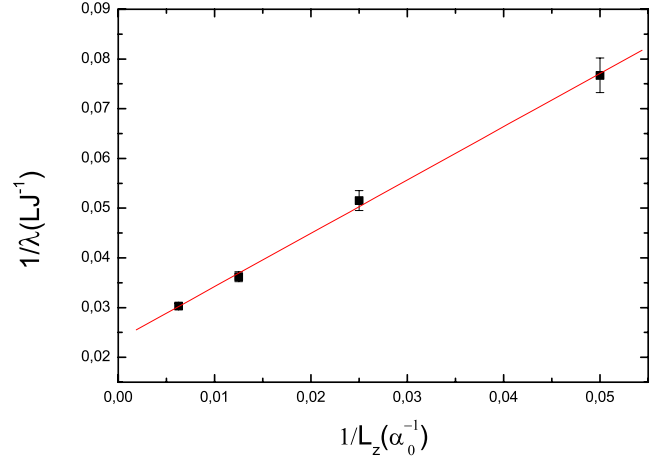


FIG. 3. (Color online) System-size dependence of inverse thermal conductivity on the inverse size. Data are shown for superlattice with rough interfaces of $2\alpha_0$ for four different sizes in z direction (20, 40, 80, and $160\alpha_0$). From this kind of graphs we can calculate the extrapolated thermal conductivity and also the phonon mean-free path for infinite size system.

for an infinite system size can be extrapolated, as well as the corresponding phonon mean-free path can be calculated. Schelling *et al.*,⁴⁵ making the assumption that the majority of the heat is carried by the acoustic modes, proposed an equation for the thermal conductivity as a function of size and the mean-free path,

$$\frac{1}{\lambda} = \frac{\alpha_0^3}{4k_B v} \left(\frac{1}{l_\infty} + \frac{4}{L_z} \right), \quad (2)$$

where k_B is the Boltzmann constant, v is the group velocity of the acoustic branch, l_∞ is the mean-free path for an infinite system, and L_z is the length of the simulation cell. This equation gives an estimation of the slope of the $1/\lambda$ function of $1/L_z$.

C. Model structures

The size effects in all directions have been examined with purpose of finding a size for which the values of the thermal conductivity and phonon mean-free path are converged. In all structures atoms are arranged on face-centered-cubic (fcc) crystalline lattice with the x , y , and z directions corresponding to the $[1,0,0]$, $[0,1,0]$, and $[0,0,1]$ directions. For the nomenclature of the characteristic length scale of the interfaces we use the term monolayer, which in an fcc lattice is equal to half of the cubic lattice parameter, $\frac{1}{2}a_0$. We studied structures with two different superlattice periods: $d_0=20a_0$ and $d_0=40a_0$. The slabs that have been simulated have sizes of $20a_0$ and $40a_0$ in x direction and $10a_0$ in the y direction while in the z direction the size was varied from 20 to $160a_0$ (Fig. 5). The system size in x direction, which is the direction of the superlattice periods, has been chosen to be of the same order of magnitude as the phonon mean-free path. Recall that the phonon mean-free path is a function of temperature. In the y direction the system size was chosen to be large enough such that it no longer has any influence on the thermal-

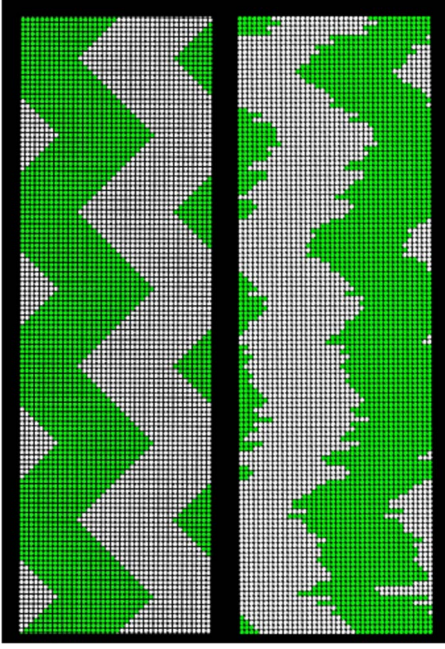


FIG. 4. (Color online) Superlattice interfaces with characteristic heights of $8a_0$, with periodic roughness (left) and random roughness (right).

conductivity results. The variation in z allows to define the extrapolated thermal conductivity for infinite (lateral) size superlattices and also to determine the phonon mean-free path, as explained above. The interfaces are oriented along the (010) crystallographic plane and the shape of interfaces is chosen to be right-isosceles triangles in the xz plane.

First, superlattices with period $20a_0$ are studied. Two kinds of interfaces are considered—interfaces with a periodic right-isosceles-triangle geometry whose height varies between 1 atomic layer or $\frac{1}{2}a_0$, a_0 , $2a_0$, $4a_0$, $6a_0$, $8a_0$, $10a_0$, and $12a_0$ for the superlattices with period $20a_0$. The $10a_0$ and $12a_0$ characteristic heights of interfaces have been studied because of the dimensions of our slab. With this roughness there is no direct way for the phonons to be transmitted thought the z direction, passing only through one type of material—interfaces with randomlike roughness to compare the effect of the shape of interfaces on the thermal conductivity. For example, for the roughness whose height is $4a_0$, the average of the characteristic height of the picks is set to $4a_0$ with variation of 25% (set arbitrary) around this value, thus the pick height varies between $3a_0$ and $5a_0$. Figure 4 represents two structures with the same roughness height: one periodic and the other random. For computational time consideration, simulation were carried out for the roughness height equal to a_0 , $4a_0$, $8a_0$, and $12a_0$.

For the structures with a double period, $40 \times 10 \times z$, we simulated the same roughness but also those of $16a_0$, $20a_0$, and $24a_0$ to examine the effect on the thermal conductivity of the ratio of superlattices period to the roughness. In Fig. 5 superlattices with smooth interfaces and with rough interfaces of $2a_0$ and $12a_0$ are presented as examples, for both superlattice periods.

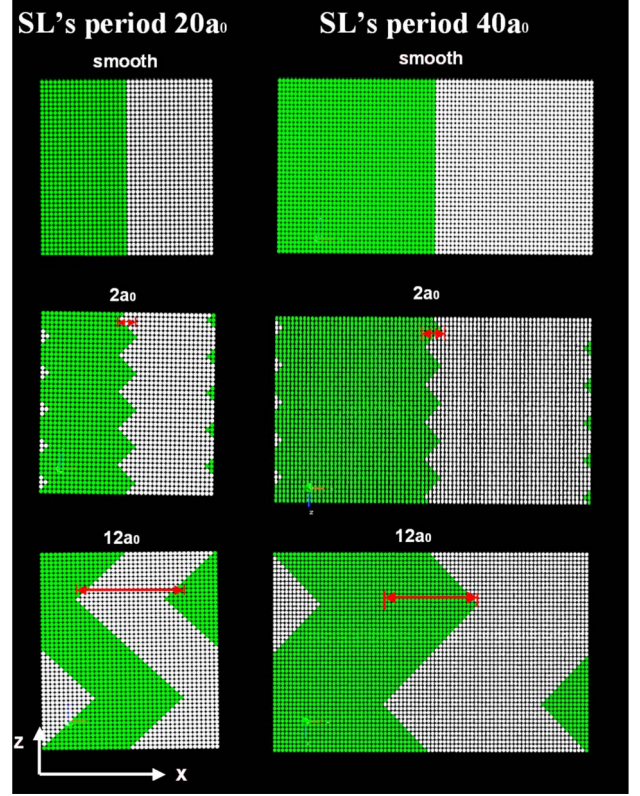


FIG. 5. (Color online) Examples of superlattices with smooth and rough interfaces studied for superlattice periods of $20a_0$ and $40a_0$. The roughness of the interfaces is on yz plane; z is the direction of the imposed temperature gradient.

III. RESULTS

A. Validation of the NEMD method

By using the methodology described in the previous section the thermal conductivity and the phonon mean-free path for the fcc bulk Lennard-Jones crystal has been calculated at a temperature of 0.15 (LJ). Thermal conductivity is equal to $\lambda_{m_1} = 73.9 \pm 1.5$ (LJ) and the phonon mean-free path $\text{PFMP}_{m_1} = 37.8a_0$ for the Lennard-Jones system with $m_1 = 1$, $\sigma = 1$, and $\epsilon = 1$. These values were obtained by extrapolation to infinite z sizes. The largest system simulated involved 2.048×10^6 atoms. The value of thermal conductivity calculated for a Lennard-Jones system can be converted in the SI system for Argon taking $\sigma = 3.40 \text{ \AA}$, $\epsilon = 1.654 \times 10^{-21} \text{ J}$, and $m_{\text{Ar}} = 6.6335 \times 10^{-26} \text{ kg}$. One obtains a value of 1.4 W/mK at a temperature of 18 K (0.15 LJ). This is in a good agreement with experimental data (1.5 to 2.5 W/mK).^{53–55} The thermal conductivity for the Lennard-Jones system with atoms of mass $m_2 = 2$ is given by

$$\begin{aligned} \lambda_{m_1} \sqrt{m_1} &= \lambda_{m_2} \sqrt{m_2} \Rightarrow \lambda_{m_2} \\ &= \frac{\lambda_{m_1}}{\sqrt{\frac{m_2}{m_1}}} = \frac{\lambda_{m_1}}{\sqrt{2}} \Rightarrow \lambda_{m_2} = 52.26 \text{ (W/mK)}. \end{aligned} \quad (3)$$

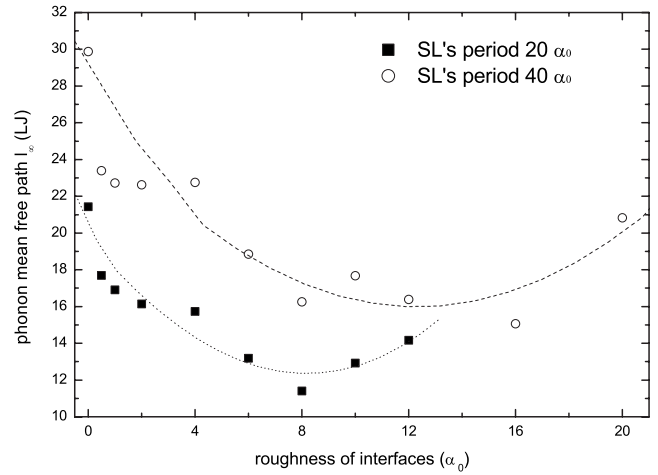
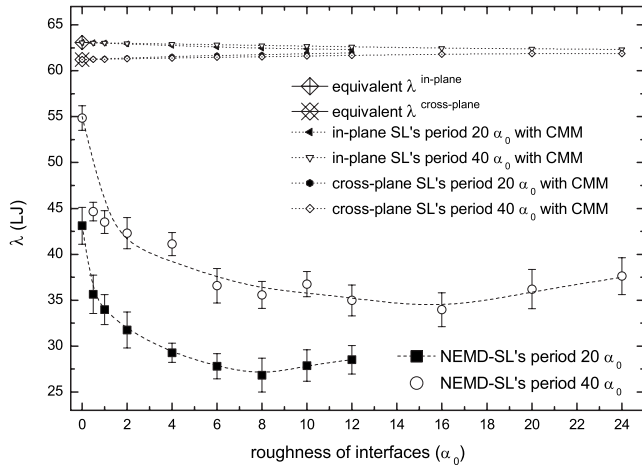


FIG. 6. (a) Thermal conductivity and (b) phonon-mean-free-path dependence on the roughness of superlattice interfaces (zero roughness denotes smooth interfaces) for the slabs with dimensions $20 \times 10 \times z$ (squares) and $40 \times 10 \times z$ (open circles). The dotted lines serve as a guide for the eyes. (SL: superlattice, CMM: continuum media method.)

B. Calculations of the thermal conductivity of superlattices with NEMD

For all the structures described above (Sec. II C), NEMD calculations have been performed. For both sets of structures ($20 \times 10 \times z, 40 \times 10 \times z$), there is a systematic decrease in the thermal conductivity and the phonon mean-free path, as the roughness is increased (Fig. 6), until a specific roughness is reached that depends on the superlattice period. For the $20 \times 10 \times z$ set of structures, the minimum occurs at a roughness of $8a_0$, while for the $40 \times 10 \times z$ set of structures it occurs at roughness of $16a_0$. Beyond the roughness at which the minimum of thermal conductivity is reached, the thermal conductivity increases. This result is unexpected and is discussed in Sec. IV. The demonstration of the minimum is actually not really obvious since the uncertainties are quite large. It would have been interesting to confirm the increasing behavior of the thermal conductivity for larger roughness height. However, for larger heights, the structures have no more interest since the fabrication would not be possible. Moreover, from a calculation point of view, larger heights would also lead to much larger systems and then consummation of huge CPU time for the simulations.

One can see the same kind of minimum also for the phonon mean-free path. Here, there is a small shift in the position of the minimum so for the $20 \times 10 \times z$ structures, the minimum occurs at $9.5a_0$ while for the $40 \times 10 \times z$ structures it occurs at a characteristic interface height of $13a_0$. Both the thermal conductivity and phonon mean-free path have higher values for the $40 \times 10 \times z$ set of structures compared to the $20 \times 10 \times z$ set [Fig. 6(a)], as expected, since the double-period superlattices have a lower density of interfaces. When the thermal conductivity reaches the minimum, its value is reduced by 40% for both $20 \times 10 \times z$ and $40 \times 10 \times z$ compared with the value obtained for the smooth interfaces.

In Fig. 7 the thermal conductivity is plotted as a function of the ratio, r , of the characteristic size of the roughness of the interfaces to the superlattice period. For the two superlattice periods ($20a_0$ and $40a_0$), the minimum in the thermal conductivity occurs at the same value of the ratio r .

The thermal-conductivity function of the roughness height for random and periodic interfaces has been calculated for a superlattice period of $20a_0$ (Fig. 8). The thermal conductivity of superlattices with random interfaces decreases monotonically in increasing roughness. This result is expected from previous literature results.^{8,27,56,57} In contrast for the periodic roughness results the thermal conductivity exhibits a minimum when the roughness height increases.

C. Calculations of the thermal conductivity of free-standing films

To enhance the interfacial effects we studied systems where one material is replaced with vacuum, i.e., free-standing films. A free surface should induce similar phenomena as an interface between two very dissimilar materials, namely, with negligible phonon transmission across the interface. Thermal conductivity for smooth films of various

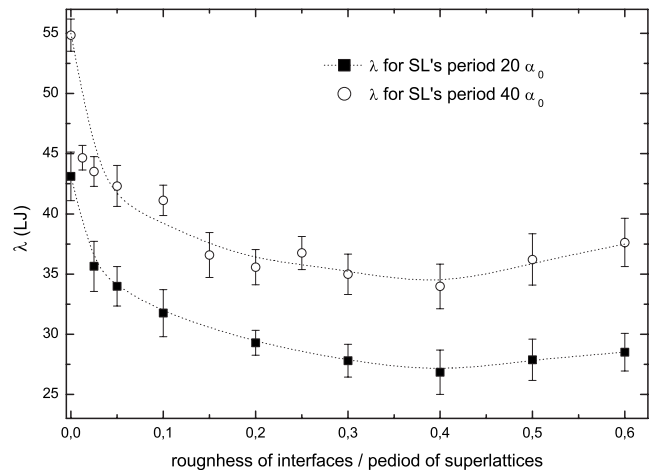


FIG. 7. In-plane thermal-conductivity dependence with the rate of roughness of superlattice interfaces with the period of superlattices ($20 \times 10 \times z$ squares and $40 \times 10 \times z$ circles). The dotted lines serve as a guide for the eyes.

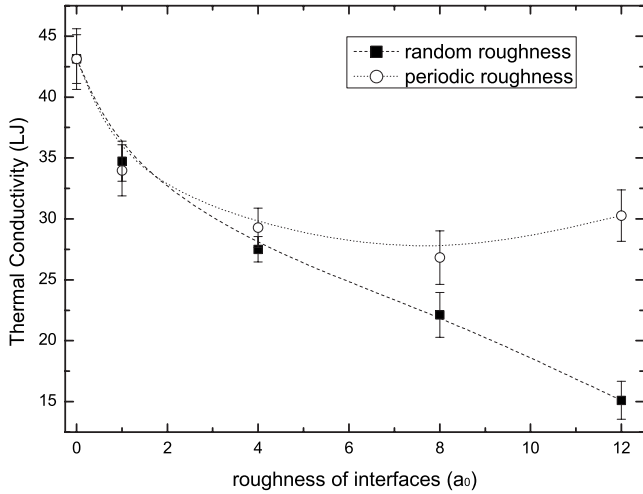


FIG. 8. Thermal conductivity function of interface roughness for superlattices of periodicity of $20a_0$. The filled squares represent the results for random roughness while the open circles are the results for interfaces with periodic roughness. The dotted lines serve as a guide for the eyes.

thicknesses have been measured and predicted.^{2,58,59} The thermal conductivity of thin films decreases when the film thickness decreases due to the increase in the scattering of phonons on free surfaces.^{60–62}

All simulations have been conducted for material 1 with mass m_1 . The slab thickness is equal to half the period of the superlattice. We chose $10a_0$ to be able to compare the results with those obtained for the superlattice with a period of $20a_0$. The smooth free surfaces and the free surfaces with roughness with characteristic sizes equal to 4, 6, 8, 10, and $12a_0$ were simulated to determine the value of the thermal conductivity (Fig. 9). The trend in the influence of the roughness on both the thermal conductivity and the phonon mean-free path is the same as for the superlattices. The minimum of the thermal conductivity occurs at the same roughness dimension ($8a_0$). The thermal conductivity and the phonon mean-free path of the free surfaces are lower than those of the

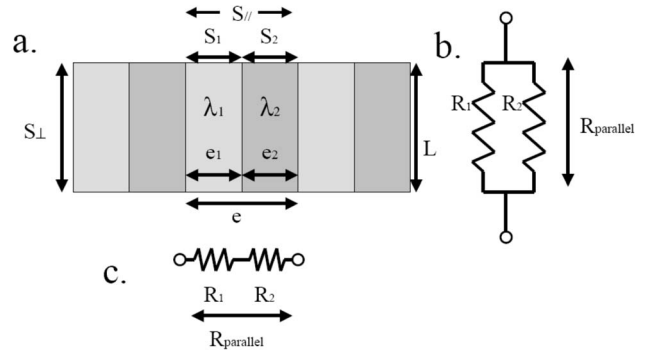
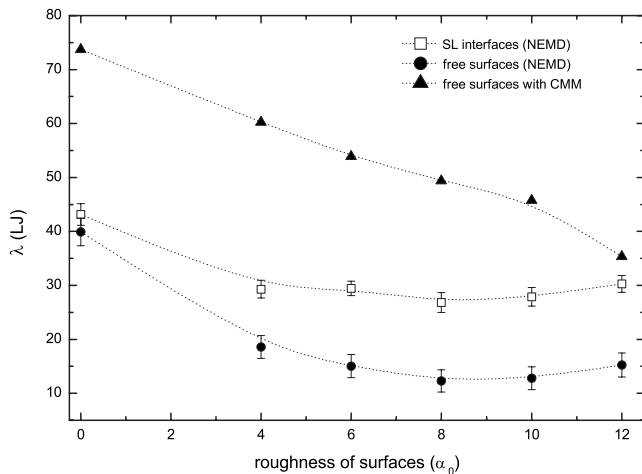


FIG. 10. Illustration of the analogy of the thermal to electrical resistance (a) the superlattice, (b) resistors in parallel for the in-plane thermal conductivity, and (c) resistors in series for the cross-plane thermal conductivity.

superlattices, which is likely due to complete phonon reflection at free interfaces.

D. Calculation of the thermal conductivity using continuum analysis

When the material is assumed to be continuous, Fourier’s law, which describes the diffusive behavior of heat carriers in matter, can be used to evaluate the thermal conductivity of the composite material assuming perfect contact between the layers. Using the analogy of the thermal to electric resistance (the schematic of the analogy of the two resistors in parallel and series is shown in Fig. 10), the equivalent thermal conductivity in the in-plane and cross-plane direction of the superlattices would be

$$\frac{1}{R_{parallel}} = \frac{1}{R_1} + \frac{1}{R_2} = \frac{\lambda_1 S_1}{L} + \frac{\lambda_2 S_2}{L}, \quad (4)$$

with

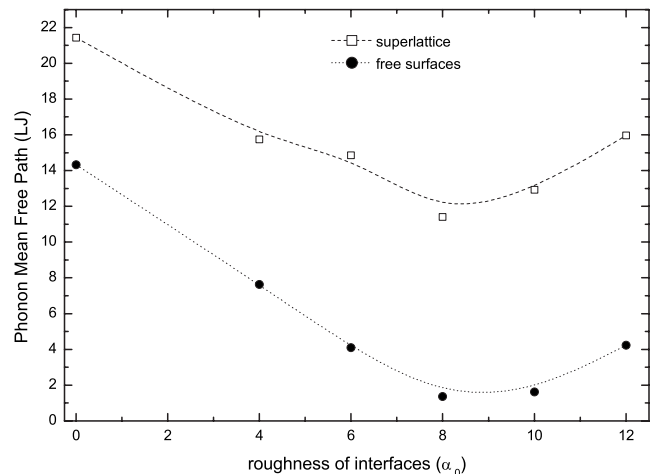


FIG. 9. (a) In-plane thermal conductivity and (b) phonon-mean-free-path function of the roughness of superlattice and of free surfaces (zero roughness denotes smooth interfaces) for the slabs with dimensions $20 \times 10 \times z$. The dotted lines serve as a guide for the eyes.

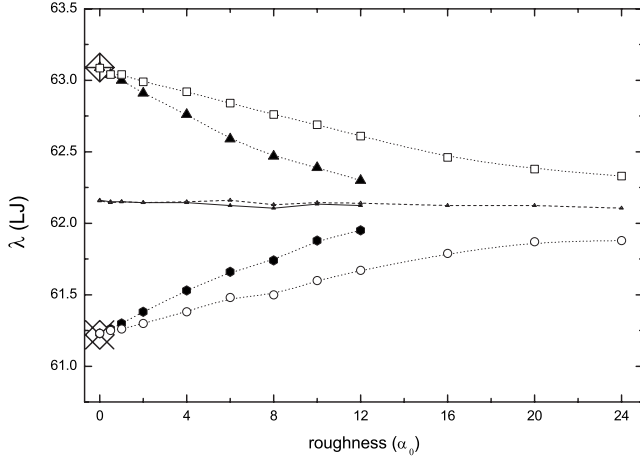


FIG. 11. In-plane and cross-plane thermal conductivity calculated with continuum-media method. For smooth interfaces, the values of thermal conductivity are extracted by the model of analogy of thermal and electrical resistance. The black triangles and the open squares are the results of the in-plane thermal conductivity for superlattice periods of 20 and $40\alpha_0$ while the black hexagons and the open circles the results of the cross-plane thermal conductivity again of superlattice periods of 20 and $40\alpha_0$ by the continuum-media method.

$$S_1 = S_2 = \frac{S_{\parallel}}{2}, \quad (5)$$

then

$$R_{parallel} = \frac{R_1 R_2}{R_1 + R_2} = \frac{L}{S} \frac{2}{\lambda_1 + \lambda_2}, \quad (6)$$

thus, the equivalent in-plane thermal conductivity is expressed by the equation

$$\lambda_{equivalent}^{in-plane} = \frac{\lambda_1 \lambda_2}{2}. \quad (7)$$

For resistors in series,

$$R_{series} = R_1 + R_2 = \frac{\epsilon 1}{\lambda_1 S_{\perp}} + \frac{\epsilon 2}{\lambda_2 S_{\perp}} = \frac{1}{2} \frac{\epsilon}{S} \frac{\lambda_1 \lambda_2}{\lambda_1 + \lambda_2} \quad (8)$$

so the equivalent cross-plane thermal conductivity is given by the formula

$$\lambda_{equivalent}^{cross-plane} = 2 \frac{\lambda_1 \lambda_2}{\lambda_1 + \lambda_2}. \quad (9)$$

By using the bulk values of thermal conductivity for masses 1 and 2 aforementioned, the equivalent in-plane thermal conductivity would be $\lambda_{equivalent}^{in-plane} = 63.09$ LJ while the equivalent thermal conductivity in the cross-plane direction would be $\lambda_{equivalent}^{cross-plane} = 61.2$ LJ. This is the value mentioned in the captions of Figs. 6(a) and 11. This value neglects the interface-scattering phenomena and should be the upper bound for the thermal conductivity of the superlattices. With the same procedure the phonon mean-free path for the two materials is $PMFP_{equivalent}^{in-plane} = 32.3a_0$ and $PMFP_{equivalent}^{cross-plane} = 31.3a_0$ ($PMFP_{m_1} = 37.8a_0$ and $PMFP_{m_2} = 26.8a_0$).

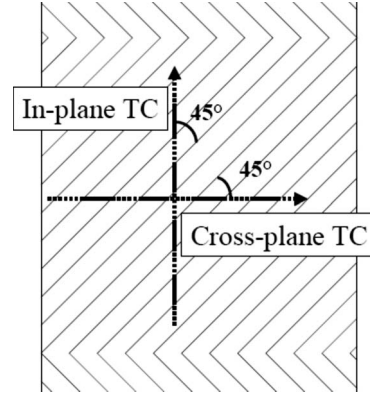


FIG. 12. Illustration of a superlattice with infinite interface roughness. The cross-plane and in-plane thermal conductivity paths are marked.

For rough interfaces, numerical solutions obtained by COMSOL multiphysics of the heat-transfer software are used to determine the equivalent thermal conductivity. In Fig. 11 the results of the equivalent thermal-conductivity dependence on roughness are shown. Treating matter as a diffusive medium (i.e., by use of the Fourier's law), the numerical solution of the differential equation of heat conduction leads to the same results as that obtained with the analytical model based on the electrical analogy for the smooth interfaces. This can be explained, as in this case the heat transfer is one dimensional so there are no heat-flux-line constrictions. In Fig. 11 there is a systematic decrease in the in-plane thermal conductivity with increasing roughness of the interfaces for both periods of superlattices. In contrast, the cross-plane thermal conductivity is increased with an increase in roughness. For the in-plane thermal conductivity the roughness-induced heat-flux-line constrictions due to the thermal-conductivity differences. For the cross-plane thermal conductivity, the presence of the roughness allows a part of the heat flux to decrease its path through the material with the lower thermal conductivity, leading to an increase in the thermal conductivity with an increase in the size of the roughness. Infinite roughness in the current study would mean imposing the temperature gradient in the direction 45° relative to the direction of the interfaces for both the in- and cross-plane cases. This can be named intraplane thermal conductivity⁶³ (Fig. 12).

IV. DISCUSSION AND CONCLUSIONS

The influence of the characteristic height of interface roughness and of the superlattice period on the in-plane thermal conductivity has been studied. The interfaces have either periodic shapes of right isosceles triangles or randomlike shapes, whose height varies from a few atomic layers to a characteristic size of the same order of magnitude as the superlattice period. Thin films with rough periodic surfaces have been also studied with the aim of determining the magnified effects introduced by the interfacial roughness.

The results obtained with the NEMD method are compared with the results obtained assuming the matter continu-

ous and diffusive for both superlattices [Fig. 6(a)] and films with free surfaces [Fig. 9(a)]. NEMD method predicts thermal conductivity which is lower by at least 60% for superlattice which periodicity is equal to $20a_0$ and 50% for superlattice period of $40a_0$ compared with the equivalent thermal conductivity, calculated with the continuum-media assumption. The continuum-media method fails to describe the thermal conductivity of superlattices when the layer thickness is of the same order of magnitude as the phonon mean-free path. The difference in the thermal conductivity for the smooth interfaces obtained with the continuum-media method and the discrete method is a combination of two effects. The first one is the phonon-confinement effect, which depends on the ratio of the superlattice period to the phonon mean-free path. With an increase in the superlattice period, the thermal conductivity increases as expected because the medium becomes more diffusive since the period size becomes larger than the phonon mean-free path [Fig. 6(b)]. The second reason is related to the thermal-boundary resistance. Although the superlattice period is decreased the density of interfaces is increased. There is no direct way to estimate quantitatively the contribution of the two effects. Finally the continuum media method predict that the cross-plane and in-plane thermal conductivity tend to the same asymptotical value when the size of the roughness increases (about 62 in LJ unit) (Fig. 11).

The thermal conductivity of superlattices with periodic rough interfaces and thin films with free periodic rough surfaces obtained with NEMDS exhibit the same trends. The phonon mean-free path and the thermal conductivity for the free surfaces are smaller compared with those of superlattices with the same roughness. This means that the phonon transmission plays an important role for the heat-transfer efficiency. In both cases, the thermal conductivity decreases when the roughness increases. It seems that the thermal conductivity reaches a minimum when the roughness increases. The detected minimum in the thermal conductivity is related to a ratio of roughness of the interfaces to superlattice period of 0.4. Concerning the variation in the superlattice period, a more pronounced decrease in the thermal conductivity was detected for superlattices with a smaller superlattice period.

A schematic of the reflection phenomena related to free surfaces with periodic roughness is illustrated in Fig. 13. The same phenomena are considered for interfaces of superlattices with periodic roughness. The main difference lies in the existence of transmission of phonons from one material to the other. Four different cases for phonon behavior can be considered, depending on the roughness of free surfaces. First of all, for smooth surfaces if one assumes that the dominant phenomenon is the specular reflection, the angle of reflection would be equal to the angle of incidence. In this case the smooth surface film would be equivalent to bulk material if the reflection would be purely specular. This is actually not the case since the thermal conductivity of the film decreases

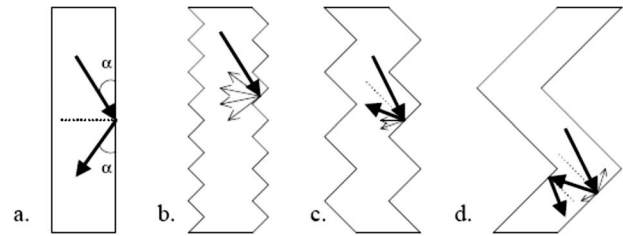


FIG. 13. Reflection cases depending on the roughness of the interfaces: (a) for smooth surfaces, (b) for surfaces with small roughness, (c) for surfaces with height of roughness comparable to the superlattice period, and (d) for surfaces, with characteristic size of surface roughness higher than the film thickness.

when the film thickness decreases (at least enough to be of the same order of magnitude as the phonon mean-free path). For rough surfaces with small roughness the reflection becomes more diffusive and the reflected phonons are distributed over a wide range of angles, which induces an additional resistance. It has been shown in the section with the results, that increasing the characteristic height of the roughness of the interfaces, there is a decrease in the thermal conductivity. For rough surfaces with high roughness there is a combination of specular and diffusive reflection. This last case shows similarities with the smooth surface but now the specular reflection gives rise to back scattering. The latter case is related to the minimum in the thermal conductivity detected for free surfaces, as well as for interfaces of superlattices. A further increase in the surface roughness leads to higher thermal conductivity. This further increase in the thermal conductivity is related to the fact that the number of interactions with surfaces is decreased and the path between each interaction is increased.

For the randomlike roughness, the monotonous decrease in the thermal conductivity in increasing the roughness's height means that the phonon behavior at the interface remains diffusive, phenomena of back scattering and specular reflection, play a secondary role here.

The variation in the ratio of interface roughness to the superlattice period can tailor the thermal properties of superlattices. The perspective is to examine the variations in the cross-plane thermal conductivity as a function of the roughness and the temperature that would affect the phonon mean-free path.

ACKNOWLEDGMENTS

This work has been conducted within the framework of a post doc financed by the CNRS to support the projects ANR-New researchers NanoMetrETher and ANR COFISIS. The authors are grateful for the use of the large computer facilities; CNRS-IDRIS and the P2CHPD of the FLCHP (Fédération Lyonnaise de Calcul Haute Performance).

*konstantinos.termentzidis@insa-lyon.fr

- ¹G. Mahan, *Thermal Conductivity of Superlattices*, *Thermal Conductivity* (Springer, New York, 2004).
- ²D. G. Cahill, W. K. Ford, K. E. Goodson, G. D. Mahan, A. Majumdar, H. J. Maris, R. Merlin, and S. R. Phillpot, *J. Appl. Phys.* **93**, 793 (2003).
- ³T. E. Sale, *Cavity and Reflector Design for Vertical Cavity Surface Emitting Lasers* (Institution of Electrical Engineers, Stevenage, 1995).
- ⁴E. K. Kim, S. I. Kwun, S. M. Lee, H. Seo, and J. G. Yoon, *Appl. Phys. Lett.* **76**, 3864 (2000).
- ⁵L. D. Hicks, T. C. Harman, and M. S. Dresselhaus, *Appl. Phys. Lett.* **63**, 3230 (1993).
- ⁶P. J. Lin-Chung and T. L. Reinecke, *Phys. Rev. B* **51**, 13244 (1995).
- ⁷Y. Ezzahri, G. Zeng, K. Fukutani, Z. Bian, and A. Shakouri, *Microelectron. J.* **39**, 981 (2008).
- ⁸B. C. Daly, H. J. Maris, K. Imamura, and S. Tamura, *Phys. Rev. B* **66**, 024301 (2002).
- ⁹S. I. Tamura, Y. Tanaka, and H. J. Maris, *Phys. Rev. B* **60**, 2627 (1999).
- ¹⁰B. Yang and G. Chen, *Phys. Rev. B* **67**, 195311 (2003).
- ¹¹G. Chen, *Phys. Rev. B* **57**, 14958 (1998).
- ¹²B. C. Daly and H. J. Maris, *Physica B* **316-317**, 247 (2002).
- ¹³S. Y. Ren and J. D. Dow, *Phys. Rev. B* **25**, 3750 (1982).
- ¹⁴G. Chen, *ASME J. Heat Transfer* **119**, 220 (1997).
- ¹⁵K. Fuchs, *Proc. Cambridge Philos. Soc.* **34**, 100 (1938).
- ¹⁶P. Hyldgaard and G. D. Mahan, *Phys. Rev. B* **56**, 10754 (1997).
- ¹⁷V. Narayanamurti, H. L. Störmer, M. A. Chin, A. C. Gossard, and W. Wiegmann, *Phys. Rev. Lett.* **43**, 2012 (1979).
- ¹⁸S. Huxtable, A. Shakouri, P. Abraham, Y. Chiu, and X. Fan, *18th International Conference on Thermoelectrics*, 1999, p. 594, <http://quantum.soe.ucsc.edu/publications/Huxtable2000.pdf>.
- ¹⁹D. W. Li, R. Y. Fan, P. Yang, and A. Majumdar, *Appl. Phys. Lett.* **83**, 3186 (2003).
- ²⁰M. V. Simkin and G. D. Mahan, *Phys. Rev. Lett.* **84**, 927 (2000).
- ²¹X. Fan, G. Zeng, C. LaBounty, J. E. Bowers, E. Croke, C. C. Ahn, S. Huxtable, A. Majumdar, and A. Shakouri, *Appl. Phys. Lett.* **78**, 1580 (2001).
- ²²C. B. Vining, W. Laskow, J. O. Hanson, R. R. Van der Beck, and P. D. Gorsuch, *J. Appl. Phys.* **69**, 4333 (1991).
- ²³R. Venkatasubramanian, *Phys. Rev. B* **61**, 3091 (2000).
- ²⁴S. M. Lee, D. G. Cahill, and R. Venkatasubramanian, *Appl. Phys. Lett.* **70**, 2957 (1997).
- ²⁵W. S. Capinski, H. J. Maris, T. Ruf, M. Cardona, K. Ploog, and D. S. Katzer, *Phys. Rev. B* **59**, 8105 (1999).
- ²⁶Y. Chen, D. Li, J. R. Lukes, Z. Ni, and M. Chen, *Phys. Rev. B* **72**, 174302 (2005).
- ²⁷K. Imamura, Y. Tanaka, N. Nishiguchi, S. Tamura, and H. Maris, *J. Phys.: Condens. Matter* **15**, 8679 (2003).
- ²⁸T. Kawamura, Y. Kangawa, and K. Kakimoto, *J. Cryst. Growth* **298**, 251 (2007).
- ²⁹S. Volz, J. B. Saulnier, G. Chen, and P. Beauchamp, *Microelectron. J.* **31**, 815 (2000).
- ³⁰D. Donadio and G. Galli, *Phys. Rev. Lett.* **102**, 195901 (2009).
- ³¹F. Marty, L. Rousseau, B. Saadany, B. Mercier, O. Français, Y. Mita, and T. Bourouina, *Microelectron. J.* **36**, 673 (2005).
- ³²Y. Mita, M. Sugiyama, M. Kubota, F. Marty, T. Bourouina, and T. Shibata, *MEMS 2006*, Istanbul Turkey, 22–26 January 2006, p. 114 (unpublished).
- ³³B. C. Daly, H. J. Maris, Y. Tanaka, and S. Tamura, *Phys. Rev. B* **67**, 033308 (2003).
- ³⁴R. Stevens, P. Norris, and L. Zhigilei, *Proceedings of the 2004 ASME International Mechanical Engineering Congress IMECE '04*, 2004, p. IMECE 2004–60334, <http://www.faculty.virginia.edu/CompMat/articles/IMECE04.pdf>.
- ³⁵P. Chantrenne, *Microscale and Nanoscale Heat Transfer* (Springer, Berlin, 2007).
- ³⁶D. Frenkel and B. Smit, *Understanding Molecular Simulation: From Algorithms to Applications* (Academic Press, San Diego, 1996).
- ³⁷D. J. Evans, *Phys. Lett.* **91A**, 457 (1982).
- ³⁸D. J. Evans, *Phys. Rev. A* **34**, 1449 (1986).
- ³⁹S. Kotake and S. Wakuri, *JSME Int. J., Ser. B* **37**, 103 (1994).
- ⁴⁰P. Chantrenne and J. L. Barrat, *Superlattices Microstruct.* **35**, 173 (2004).
- ⁴¹P. Chantrenne and J. L. Barrat, *ASME J. Heat Transfer* **126**, 577 (2004).
- ⁴²F. Müller-Plathe, *J. Chem. Phys.* **106**, 6082 (1997).
- ⁴³R. J. Stevens, L. V. Zhigilei, and P. M. Norris, *Int. J. Heat Mass Transfer* **50**, 3977 (2007).
- ⁴⁴R. H. H. Poetzsch and H. Böttger, *Phys. Rev. B* **50**, 15757 (1994).
- ⁴⁵P. K. Schelling, S. R. Phillpot, and P. Keblinski, *Phys. Rev. B* **65**, 144306 (2002).
- ⁴⁶E. Landry, A. McGaughey, and M. Hussein, *ASME paper HT2007–32152, ASME 2007 Summer Heat Transfer Conference*, Vancouver, BC, July 2007 (unpublished).
- ⁴⁷S. S. Mahajan, G. Subbarayan, and B. G. Sammakia, *Phys. Rev. E* **76**, 056701 (2007).
- ⁴⁸<http://lammps.sandia.gov/>
- ⁴⁹S. Plimpton, *J. Comput. Phys.* **117**, 1 (1995).
- ⁵⁰S. Plimpton, R. Pollock, and M. Stevens, in *Proceedings of the Eighth SIAM Conference on Parallel Processing for Scientific Computing*, Minneapolis, MN, 1997 (unpublished).
- ⁵¹E. T. Swartz and R. O. Pohl, *Rev. Mod. Phys.* **61**, 605 (1989).
- ⁵²J. R. Lukes, D. Y. Li, X. G. Liang, and C. L. Tien, *ASME J. Heat Transfer* **122**, 536 (2000).
- ⁵³G. K. White and S. B. Woods, *Philos. Mag.* **3**, 785 (1958).
- ⁵⁴B. K. Agrawal and G. S. Verma, *Phys. Rev.* **126**, 24 (1962).
- ⁵⁵D. K. Christen and G. L. Pollack, *Phys. Rev. B* **12**, 3380 (1975).
- ⁵⁶E. S. Landry and A. J. H. McGaughey, *Phys. Rev. B* **79**, 075316 (2009).
- ⁵⁷M. N. Touzelbaev, P. Zhou, R. Venkatasubramanian, and K. E. Goodson, *J. Appl. Phys.* **90**, 763 (2001).
- ⁵⁸S. Moon, M. Hatano, M. Lee, and C. P. Grigoropoulos, *Int. J. Heat Mass Transfer* **45**, 2439 (2002).
- ⁵⁹B. L. Zink, B. Revaz, J. J. Cherry, and F. Hellman, *Rev. Sci. Instrum.* **76**, 024901 (2005).
- ⁶⁰G. Chen, *Phonon Heat Conduction in Low-Dimensional Structures, Semiconductors and Semimetals, Recent Trends in Thermoelectric Materials Research* (Academic Press, San Diego, 2001).
- ⁶¹D. Z. Chen, A. Narayanaswamy, and G. Chen, *Proceedings of IMECE2005*, November 5–11, 2005, Orlando, Florida, USA, <http://web.mit.edu/nanoengineering/publications/PDFs/IMECE2-5-83051.pdf>.
- ⁶²D. Terris, K. Joulain, D. Lemonnier, D. Lacroix, and P. Chantrenne, *Int. J. Therm. Sci.* **48**, 1467 (2009).
- ⁶³I. Vekhter and A. Vorontsov, *Phys. Rev. B* **75**, 094512 (2007).